

Room Temperature Thermoelectric Properties of Isostructural Selenides Ta₂PdS₆ and Ta₂PdSe₆

Akitoshi Nakano^{1*}, Urara Maruoka¹, Fumiaki Kato¹, Hiroki Taniguchi¹ and Ichiro Terasaki¹

¹*Department of Physics, Nagoya University, Nagoya 464-8602, Japan*

We have measured thermoelectric properties of Ta₂PdX₆ (X=S, Se) around room temperature using single crystal samples. We find that the power factor of Ta₂PdX₆ is relatively high from middle-low to room temperatures, and notably Ta₂PdSe₆ shows the largest power factor among thermoelectric materials with an electrical conductivity of 10⁻² Ωcm at 300 K. Ta₂PdS₆ will be a possible candidate for a Peltier cooling material if the lattice thermal conductivity is reduced by chemical substitution.

Transition-metal chalcogenides have attracted much attention due to their unique physical properties arising from their low-dimensionality. Charge density wave¹⁾, superconductivity²⁾, and topologically nontrivial electronic phases³⁾ in binary transition-metal dichalcogenides have been one of the central issues of the condensed matter physics. Ternary transition-metal chalcogenides with strong one-dimensionality (1D) also attract keen interests due to their exotic physical properties. For instance, a quasi 1D telluride Ta₄SiTe₄ and its sister compounds show good thermoelectric properties from middle-low to room temperatures⁴⁾⁻⁶⁾. Another quasi 1D selenide Ta₂NiSe₅ is a candidate of the excitonic insulator (EI)⁷⁾⁻⁹⁾, which has been pursued for long time from its theoretical prediction in the 1960s.

Ta₂PdX₆ (X=S, Se), which was synthesized in 1985¹⁰⁾, is yet another 1D ternary transition-metal chalcogenide. This compound crystallizes in the monoclinic structure with the space

group $C2/m$. Ta_2PdX_6 has a layered crystal structure, where the square planar PdX_4 and face-shared TaX_6 prisms form 1D chains along the b -axis direction as shown in Fig.1(a). Except for superconductivity with $T_c = 4.5$ K in $(C_2H_8N_2)_yTa_2PdSe_6$ ¹¹⁾ and ultrahigh photo-responsibility in atomic layer Ta_2PdS_6 ¹²⁾, fundamental bulk transport properties of Ta_2PdX_6 have not been investigated yet.

In this letter, we focus on the transport properties of Ta_2PdX_6 . The chemical formula and the characteristic 1D crystal structure are quite similar to the EI candidate Ta_2NiSe_5 , which we have investigated by means of structural analyses¹³⁾¹⁴⁾ and transport measurement¹⁵⁾¹⁶⁾ thus far. This structural similarity suggests that Ta_2PdX_6 may be on the verge of the excitonic instability. Since the EI is predicted to realize in a semiconductor or semimetal, the bandgap $|E_g|$ of which are smaller than the binding energy between an electron and a hole¹⁷⁾⁻²²⁾, the transport measurements are essential to explore EIs. In this context, we conducted transport measurements on Ta_2PdX_6 to compare with Ta_2NiSe_5 . Although no reminiscent signs of an excitonic phase transition was observed in Ta_2PdX_6 , we instead found that Ta_2PdX_6 shows relatively large thermoelectric power factor from middle-low to room temperatures.

High-quality single crystals of Ta_2PdX_6 ($X = S, Se$) were grown by means of I_2 vapor transport. Powders of tantalum (99.9%), palladium (99.9%), and sulfur/selenium (99.999%) were loaded into an evacuated quartz tube with an I_2 concentration of ~ 3 mg/cm³. Then, a temperature difference of 145 °C between 875 °C and 730 °C in a three-zone furnace was used for crystal growth for 4 days. Shiny silver needle-like single crystals of Ta_2PdX_6 (Figs.1(b) and (c)) are obtained at the cold end of the tube. The crystals are identified by single crystal X-ray diffraction. We confirmed that the needle direction is along the crystal b -axis.

Transport properties along the b -axis direction, including resistivity, thermopower, and Hall resistivity, were measured using PPMS (Quantum Design). The resistivity was measured by a four-probe method using gold wires with 20 μ m diameters and silver paste. The thermopower

was measured with a steady state and the two-probe technique. The sample bridged two separated copper heat baths, and the resistance heater created a temperature difference between the two heat baths, which was monitored through a copper-constantan differential thermocouple. The Hall resistivity was measured by sweeping magnetic field from -7 to 7 T at constant temperatures. The signal was collected using ΔR mode of a nano-ohmmeter LR-700 (LINEAR RESEARCH INC). In-plane thermal diffusivity was measured with a home-made measurement station based on an ac calorimetric method. The details will be published in a separate paper.

Figure 2(a) shows the temperature dependence of the resistivity and the Seebeck coefficient of Ta_2PdS_6 . The resistivity is relatively low, $8 \text{ m}\Omega\text{cm}$ at 300 K . As temperature decreases, the resistivity exponentially increases. The activation energy estimated from the Arrhenius plot is $\sim 40 \text{ meV}$, indicating a narrow gap semiconductor state. The Seebeck coefficient is negative and as large as $450 \text{ }\mu\text{V/K}$ at 300 K . The absolute value of Seebeck coefficient increases to $600 \text{ }\mu\text{V/K}$ as temperature decreases down to 100 K .

The inset of Fig.2(a) shows the field dependence of the Hall resistivity at 100 K . The value of the Hall coefficient at 100 K is $-1.4 \text{ cm}^3/\text{C}$. The negative sign is consistent with the sign of the Seebeck coefficient. If we assume a single carrier model, the estimated electron density and carrier mobility R_H/ρ at 100 K are a low value of $4.6 \times 10^{18} \text{ cm}^{-3}$ and a relatively high value of $60 \text{ cm}^2/\text{Vs}$, respectively.

Figure 2(b) shows the temperature dependence of the resistivity and the Seebeck coefficient of Ta_2PdSe_6 . In contrast to the semiconducting resistivity of Ta_2PdS_6 , Ta_2PdSe_6 shows metallic resistivity which decreases linearly upon cooling. The drastic change from semiconductor to metal depending on iso-valent X may imply that the band structure near the Fermi level on Ta_2PdX_6 is significantly affected by the difference of electronegativity between sulfur and selenium. At room temperature, the sign of the Seebeck coefficient is negative and smaller than the Seebeck coefficient for Ta_2PdS_6 . As temperature decreases, the Seebeck coefficient goes to

zero around 100 K, indicating the sign change.

The field dependence of the Hall resistivity at 120 K is shown in the inset of Fig. 2(b). Contrary to Ta₂PdS₆, the sign of the Hall coefficient at 120 K is positive, indicating coexistence of electrons and holes. If we employ a two carrier model, the Hall coefficient R_H can be written as

$$R_H = \frac{p\mu_h^2 - n\mu_e^2}{e(p\mu_h + n\mu_e)^2}. \quad (1)$$

where, n (p), e , and $\mu_{e(h)}$ are the concentration of electrons (holes), the element charge, and the carrier mobility of the electron (hole), respectively. Imposing a semimetallic condition $n = p$, we can rewrite equation (1) as

$$R_H = \frac{\mu_h - \mu_e}{ne(\mu_h + \mu_e)}. \quad (2)$$

Since the resistivity can be written as

$$\rho = \frac{1}{ne(\mu_h + \mu_e)}, \quad (3)$$

using equation (2) and (3) we can obtain the difference between the carrier mobility of electrons and holes as

$$R_H/\rho = \mu_h - \mu_e \quad (4)$$

Using equation (4) R_H/ρ is estimated to be ~ 400 cm²/Vs, indicating a high and asymmetric carrier mobility in Ta₂PdSe₆.

Figure 2(c) shows the thermoelectric power factor of Ta₂PdX₆ as a function of temperature. The power factor S^2/ρ is a measure of the electric power converted from thermal energy across a temperature difference of 1 K. Thus, a material with higher power factor is demanded to generate more electricity. We also plot the power factor of an EI candidate Ta₂NiSe₅¹⁵⁾, together with pristine Bi₂Te₃²³⁾ that is a commercially available thermoelectric material. As shown in Fig. 2(c), Ta₂PdX₆ shows higher power factor than Ta₂NiSe₅ in spite of the structural similarity. Furthermore, the power factor of Ta₂PdS₆ is larger than pristine Bi₂Te₃ in a wide temperature

range from 100 to 300 K.

Figure 3 shows the room temperature power factor of various materials²⁴⁾ plotted as a function of resistivity. We find that the power factor of Ta_2PdX_6 is in a top level among thermoelectric materials reported thus far, and especially Ta_2PdS_6 shows the largest power factor among the materials which have resistivity around $10^{-2} \Omega\text{cm}$. In the case of semimetallic Ta_2PdSe_6 , the relatively large power factor stems from the high electric conductivity due to high carrier mobility, whereas in the case of semiconductor Ta_2PdS_6 , the large power factor comes from the large Seebeck coefficient due to existence of the bandgap.

Note that the power factor of Ta_2NiSe_5 is three orders magnitude smaller than that of Ta_2PdS_6 at 300 K. Since their resistivity is of the same order, the small power factor of Ta_2NiSe_5 is due to the smaller Seebeck coefficient of Ta_2NiSe_5 than Ta_2PdS_6 . The smaller Seebeck coefficient in spite of the larger bandgap $\sim 160 \text{ meV}$ ⁹⁾ indicates that the significant compensation between the Seebeck coefficient of electrons and holes. According to the recent Hall resistivity measurements, the difference between the carrier mobility of electrons and holes of Ta_2NiSe_5 is smaller than $20 \text{ cm}^2/\text{Vs}$ ²⁵⁾ in a wide temperature range, whereas Ta_2PdS_6 shows a larger R_H/ρ of $60 \text{ cm}^2/\text{Vs}$. This suggests that the small difference between the carrier mobility of electrons and holes plays a role for the compensation of the Seebeck coefficient in Ta_2NiSe_5 . Instead, the almost equal carrier mobility of electrons and holes may favor the excitonic bound state of electrons and holes in Ta_2NiSe_5 .

Finally, we evaluate the dimensionless figure of merit $ZT (= S^2/\rho\kappa)$ of Ta_2PdX_6 which is a measure of energy-conversion efficiency. Combining the thermal diffusivity measured by ac calorimetric method with the heat capacity assumed by the Dulong-Petit law, κ is determined to be 14 W/mK for Ta_2PdS_6 and 17 W/mK for Ta_2PdSe_6 , as summarized in Table.1. Employing these κ values, we evaluate ZT to be 6.4×10^{-2} and 2.1×10^{-2} , for Ta_2PdS_6 and Ta_2PdSe_6 , respectively, which are as large as other sulfides²⁶⁾ and far below Bi_2Te_3 for $ZT = 1$ ²⁷⁾. This is

due to 15 times higher κ of Ta_2PdX_6 than that of Bi_2Te_3 ²⁷⁾. Applying the Wiedemann-Franz law to the ρ data, the electron contribution to the thermal conductivity is negligible for Ta_2PdS_6 . The evaluated phonon mean free path at 300 K for Ta_2PdS_6 is about 5 ~ 10 nm which is longer than the lattice constant. Thus, if we can simultaneously suppress the lattice thermal conductivity and resistivity by chemical substitution, Ta_2PdS_6 can be a potential thermoelectric material.

We conducted transport measurements on Ta_2PdX_6 (X=S, Se) which has a similar characteristic one-dimensional crystal structure to an excitonic insulator candidate Ta_2NiSe_5 . From the resistivity and the Seebeck coefficient measurements, we reveal that Ta_2PdS_6 is a semiconductor with a narrow gap of 40 meV, whereas Ta_2PdSe_6 is a good metal. The thermoelectric power factor is relatively large for the both compounds. Especially, Ta_2PdS_6 shows the largest power factor among the materials which have resistivity around 10^{-2} Ωcm . The evaluated dimensionless figure of merit of Ta_2PdX_6 is as large as other sulfides. If we can simultaneously suppress the lattice thermal conductivity and resistivity by chemical substitution, Ta_2PdS_6 can be a potential thermoelectric material.

Acknowledgments

This work was partly supported by Nanotechnology Platform Program (Molecule and Material Synthesis) of the Ministry of Education, Culture, Sports, Science and Technology (MEXT), Japan, Grant Number JPMXP09S20NU0029. This work is partially supported by Kakenhi Grant Nos. 17H06136, 19H05791 and 20K20898 of Japan.

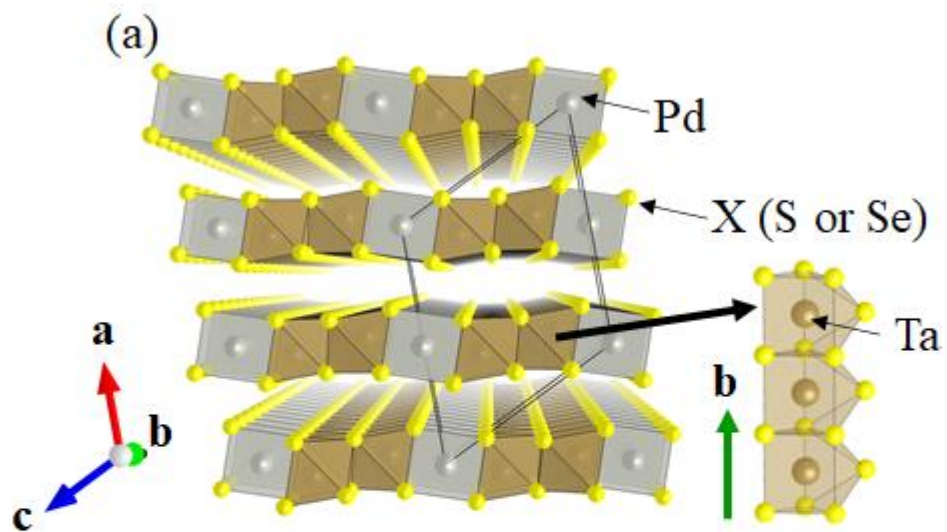
*E-mail: nakano.akitoshi@f.mbox.nagoya-u.ac.jp

1) J.A. Wilson, F. J. Di Salvo and S. Mahajan, Adv. Phys. **24** 117-201 (1975).

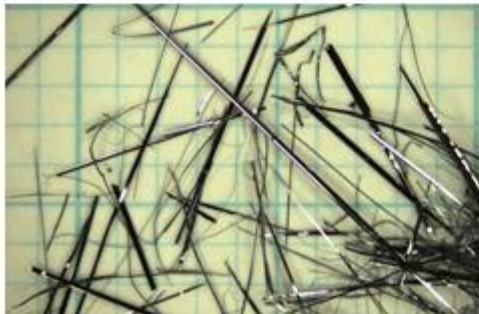
- 2) E. Morosan, H. W. Zandbergen, B. S. Dennis, J. W. G. Bos, Y. Onose, T. Klimczuk, A. P. Ramirez, N. P. Ong, and R. J. Cava, *Nature Physics*, **2**, 544-550 (2006).
- 3) H.-J. Noh, J. Jeong, E.-J. Cho, K. Kim, B. I. Min, and B.-G. Park, *Phys. Rev. Lett.* **119**, 016401 (2017)
- 4) T. Inohara, Y. Okamoto, Y. Yamakawa, A. Yamakage, and K. Takenaka, *Appl. Phys. Lett.* **111**, 183901 (2017)
- 5) Y. Okamoto, T. Wada, Y. Yamakawa, T. Inohara, and K. Takenaka, *Appl. Phys. Lett.* **112**, 173905 (2018)
- 6) Y. Okamoto, Y. Yoshikawa, T. Wada, and K. Takenaka, *Appl. Phys. Lett.* **115**, 043901 (2019)
- 7) Y. Wakisaka, T. Sudayama, K. Takubo, T. Mizokawa, M. Arita, H. Namatame, M. Taniguchi, N. Katayama, M. Nohara, and H. Takagi, *Phys. Rev. Lett.* **103**, 026402 (2009).
- 8) T. Kaneko, T. Toriyama, T. Konishi, and Y. Ohta, *Phys. Rev. B* **87**, 035121 (2013).
- 9) Y. F. Lu, H. Kono, T. I. Larkin, A. W. Rost, T. Takayama, A. V. Boris, B. Keimer, and H. Takagi, *Nat. Commun.* **8**, 14408 (2017).
- 10) D. A. Keszler, P. J. Squattrito, N. E. Brese, J. A. Ibers, S. Maoyu, and L. Jiaxi *Inorg. Chem.* **24** 3063-3067 (1985).
- 11) S. Nakamura, T. Noji, T. Hatakeda, K. Sato, T. Kawamata, M. kato, and Y. Koike, *Journal of Physics: Conf. Series* **969**, 012076 (2018)
- 12) P. Yu, Q. Zeng, C. Zhu, L. Zhou, W. Zhao, J. Tong, Z. Liu, and G. Yang, *Adv. Mater.* **2005607** (2020).
- 13) A. Nakano, K. Sugawara, S. Tamura, N. Katayama, K. Matsubayashi, T. Okada, Y. Uwatoko, K. Munakata, A. Nakao, H. Sagayama, R. Kumai, K. Sugimoto, N. Maejima, A. Machida, T. Watanuki, and H. Sawa, *IUCrJ*, **5**, 158 (2018).
- 14) A. Nakano, T. Hasegawa, S. Tamura, N. Katayama, S. Tsutusi, and H. Sawa, *Phys. Rev. B*, **98**, 045139 (2018).

- 15) A. Nakano, T. Nagai, N. Katayama, H. Sawa, H. Taniguchi, and I. Terasaki, *J. Phys. Soc. Jpn.* 88, 113706 (2019)
- 16) A. Nakano, U. Maruoka, H. Taniguchi, and I. Terasaki, *J. Phys. Soc. Jpn.* 89, 045001 (2020)
- 17) L. V. Keldysh, and Y. V. Kopeav, *Sov. Phys. Solid State* 6, 2219 (1965).
- 18) J. Des Cloizeaux, *J. Phys. Chem. Solids* 26, 259 (1965).
- 19) D. Jérôme, T. M. Rice, and W. Kohn, *Phys. Rev.* 158, 462 (1967).
- 20) B. I. Halperin, and T. M. Rice, *Rev. Mod. Phys.* 40, 755 (1968).
- 21) B. I. Halperin, and T. M. Rice, *Solid State Physics*, Vol. 21 (Academic Press, New York, 1968) p. 115.
- 22) W. Kohn, *Phys. Rev. Lett.* 19, 439 (1967).
- 23) J. W. G. Bos, H. W. Zandbergen, M. -H. Lee, N. P. Ong, and R. J. Cava *Phys. Rev. B* 75, 195203 (2007).
- 24) M. W. Gaultois, T. D. Sparks, C. K. H. Borg, R. Seshadri, W. D. Bonificio, and D. R. Clarke *Chem. Mater.* 25, 15, 2911-2920 (2013).
- 25) H. Arima, Y. Naito, K. Kudo, N. Katayama, H. Sawa, M. Nohara, Y. Lu, K. Kitagawa, H. Takagi, Y. Uwatoko, K. Matsubayashi *JPS Conf. Proc.* 30, 011031 (2020).
- 26) K. Suekuni, K. Tsuruta, M. Kunii, H. Nishiate, E. Nishibori, S. Maki, M. Ohta, A. Yamamoto, and M. Koyano, *J. Appl. Phys.* 113, 043712 (2013).
- 27) H. J. Goldsmid *Materials* 7, 2577 (2014).

Fig.1



(b) Ta_2PdS_6



(c) Ta_2PdSe_6



Figure 1. (Color online) (a) Crystal structure of Ta_2PdX_6 . The right-side figure shows the TaX_6 prismatic coordination arranged along b -axis sharing the faces. Photographic images of single crystals of (b) Ta_2PdS_6 and (c) Ta_2PdSe_6 .

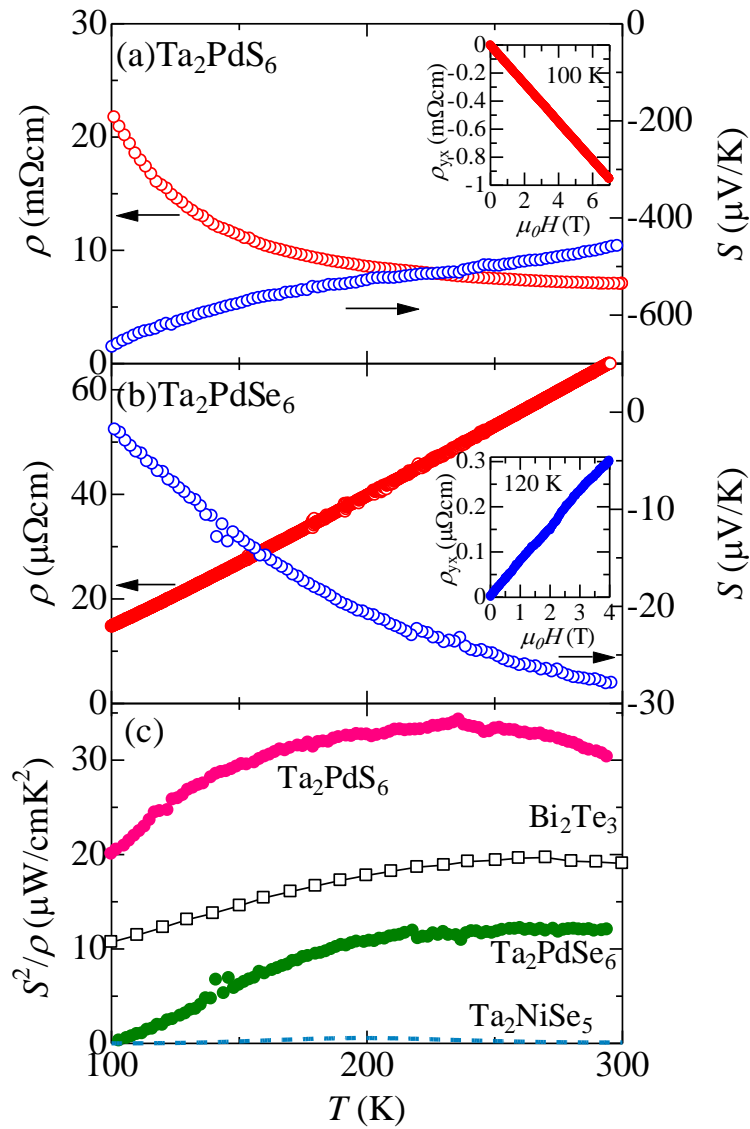


Figure 2. (Color online) Temperature dependence of the resistivity and the Seebeck coefficient of (a) Ta₂PdS₆ and (b) Ta₂PdSe₆. In the inset of (a) and (b) the Hall resistivity for Ta₂PdS₆ at 100 K and Ta₂PdSe₆ at 120 K are also shown. (c) Temperature dependence of the power factor S^2/ρ of Ta₂PdX₆. The power factor of Bi₂Te₃²³⁾ and Ta₂NiSe₅¹⁵⁾ is also shown for comparison.

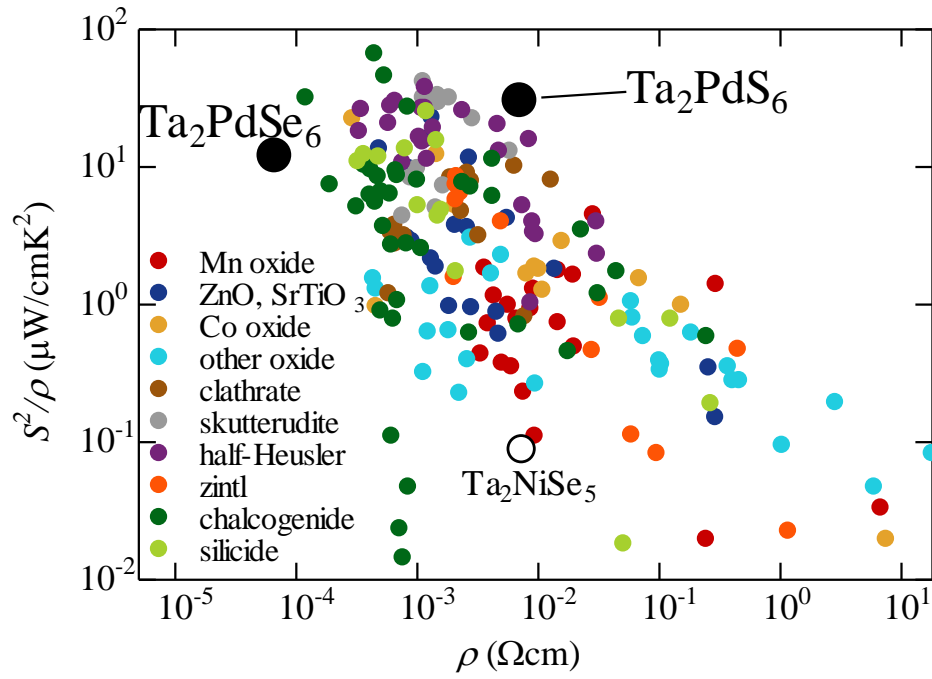


Figure 3. (Color online) Comparison of the power factor of Ta_2PdX_6 ($X=\text{S}, \text{Se}$) with other thermoelectric materials. The data points except for Ta_2PdX_6 and Ta_2NiSe_5 are obtained from Materials Research Laboratory database of 300 K²⁴).

Table 1. Summary of the used parameters to determine the thermal conductivity at 300 K.

sample	Thermal diffusivity (m ² /s)	Heat capacity (J/molK)	Density (mol/m ³)	Thermal conductivity (W/mK)	<i>ZT</i>
Ta ₂ PdS ₆	6.7×10 ⁻⁶	2.2×10 ²	8.5×10 ³	14	6.4×10 ⁻²
Ta ₂ PdSe ₆	8.9×10 ⁻⁶	2.2×10 ²	9.6×10 ³	17	2.1×10 ⁻²